Rain-Profiling Algorithm for the TRMM Precipitation Radar

TOSHIO IGUCHI

Global Environment Division, Communications Research Laboratory, Koganei, Tokyo, Japan

TOSHIAKI KOZU

Department of Electronic and Control Systems Engineering, Shimane University, Matsue, Japan

ROBERT MENEGHINI

NASA Goddard Space Flight Center, Greenbelt, Maryland

JUN AWAKA

Department of Information Science, Hokkaido Tokai University, Sapporo, Japan

KEN'ICHI OKAMOTO

Department of Aerospace Engineering, Osaka Prefecture University, Sakai, Japan

(Manuscript received 24 October 1999, in final form 28 April 2000)

ABSTRACT

This paper describes the Tropical Rainfall Measuring Mission (TRMM) standard algorithm that estimates the vertical profiles of attenuation-corrected radar reflectivity factor and rainfall rate. In particular, this paper focuses on the critical steps in the algorithm. These steps are attenuation correction, selection of the default drop size distribution model including vertical variations, and correction for the nonuniform beam-filling effect. The attenuation correction is based on a hybrid of the Hitschfeld–Bordan method and a surface reference method. A new algorithm to obtain an optimum weighting function is described. The nonuniform beam-filling problem is analyzed as a two-dimensional problem. The default drop size distribution model is selected according to the criterion that the attenuation estimates derived from the model and the independent estimates from the surface reference with the nonuniform beam-filling correction are consistent for rain over ocean. It is found that the drop size distribution models that are consistent for convective rain over ocean are not consistent over land, indicating a change in the size distributions associated with convective rain over land and ocean, respectively.

1. Introduction

The precipitation radar (PR) on the Tropical Rainfall Measuring Mission (TRMM) satellite enables capture of the three-dimensional storm structure over the ocean and land where no radar data of this kind was available before. The vertical and horizontal distributions of rain are the data wanted by many users to investigate not only storm structures but also global circulation models. To obtain the unbiased three-dimensional rain structure, however, it is essential to correct for the attenuation effect before radar echo intensities are converted into rainfall rates, because the radar echo at the PR frequency of 13.8 GHz suffers from significant attenuation. How to convert the attenuation-corrected radar echoes into rainfall rates is another important issue.

This paper describes the TRMM standard algorithm that estimates the vertical profiles of attenuation-corrected radar reflectivity factor and rainfall rate. This algorithm is designated as 2A25 in the TRMM project. The algorithm has been revised several times. This paper describes version 5.53 of 2A25, which has been used to generate the operational version-5 products since November 1999.

Instead of the procedural details of the processing flow, this paper focuses on the critical steps in the algorithm that include attenuation correction, selection of the default drop size distribution model, and correction for nonuniform beam-filling effects. The overall processing flow is outlined in the next section.

Corresponding author address: Toshio Iguchi, Global Environment Division, Communications Research Laboratory, 4-2-1 Nukui Kitamachi, Koganei, Tokyo 184-8795, Japan.
E-mail: iguchi@crl.go.jp

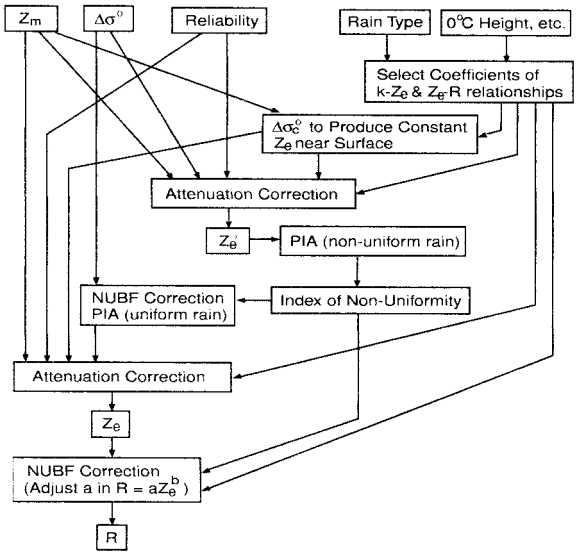

FIG. 1. Simplified flow chart of the 2A25 algorithm.

2. Outline of the algorithm

The TRMM satellite is a non–Sun-synchronous satellite orbiting at about 350 km above the surface. The PR instrument observes the swath of 220 km with 49 beams every 0.6 s. Each beamwidth is about 0.7°, and the footprint diameter is approximately 4.3 km at nadir. The pulse width of 1.67 μs corresponds to a range resolution of 250 m.

The 2A25 algorithm estimates the true effective reflectivity factor Z_e at 13.8 GHz at each radar resolution cell from the measured vertical profiles of reflectivity factor Z_m. The rainfall rate R is then calculated from the estimated Z_e.

A simplified flow chart of the 2A25 algorithm is shown in Fig. 1. The input data files are 1C21, 2A21, and 2A23. The main data from 1C21 are the measured radar Z_m profiles and miscellaneous rain height information. 2A21 provides 2A25 with an estimate of path attenuation and its reliability as derived from the apparent decrease of the surface cross section in rain relative to that measured in rain-free areas. Algorithm 2A23 provides rain type, brightband height, and freezing-height information. The designations of the TRMM satellite algorithms and the contents of the corresponding products are described in Simpson et al. (2000) and Kummerow et al. (2000).

The 2A25 algorithm first defines the region for processing, selecting only those range gates between the rain top and the lowest height above the surface that is free from surface clutter. The current algorithm does not use any data below the surface, that is, the mirror image. The brightband height and climatological surface atmospheric temperature are used to define the regions where the hydrometeors are primarily liquid (water), solid (ice), and mixed phase. The initial values of the coefficients in the k–Z_e and Z_e–R relationships at different altitudes are defined accordingly. Here k denotes the specific attenuation.

The attenuation correction is based on a hybrid of the surface reference method and the Hitschfeld–Bordan method (Iguchi and Meneghini 1994). The coefficient α in the k–Z_e relationship $k = \alpha Z_e^{\beta}$ is adjusted in such a way that the path-integrated attenuation (PIA) estimated from the measured Z_m profile by the Hitschfeld–Bordan method matches the estimate of PIA from the surface reference.

The attenuation-corrected Z_e at all ranges are calculated by using the Hitschfeld–Bordan method with the modified α. This α-adjustment method assumes that the discrepancy between the PIA estimate from the surface reference and that from the measured Z_m profile can be attributed to an inappropriate initial choice of α primarily because of differences between the assumed and actual raindrop size distribution. It assumes that the radar is properly calibrated and that Z_m is unbiased. Effects of a bias in Z_m are discussed later.

The attenuation correction procedure requires two processing cycles. In the first cycle, correction is made without taking the nonuniform beam-filling effect into account. From these attenuation-corrected profiles, PIA at each angle bin is calculated. The low-resolution variability of PIA for a given angle bin is calculated from the PIAs at the angle bin in question and the eight surrounding angle bins. The high-resolution variability of the PIA, that is, the horizontal variation within the radar resolution cell, is then estimated from the variability of the low-resolution PIAs (Kozu and Iguchi 1999). An index of nonuniformity is defined as the normalized standard deviation of the high-resolution path attenuations, where the normalized standard deviation, or coefficient of variation, is the ratio of the standard deviation to the mean. The nonuniformity index is used to change the path attenuation derived from the surface reference technique to that that would be observed if the rain were distributed uniformly in a plane perpendicular to the range direction within each radar beam. In the second processing cycle, the modified PIA is used to compute the Z_e profile that is written to the output file.

The rainfall estimates are calculated from the Z_e profiles by using a power law: $R = aZ_e^b$ in which the parameters a and b are both functions of the rain type and the heights of the 0°C isotherm and storm top. Effects of rain type, presence or absence of a bright band, the phase state, the temperature, and the difference in terminal velocity from changes in the air density are taken into account. Moreover, the initial values of a and b are modified according to the adjustment in α so that the k–Z_e and Z_e–R relations are consistent with the assumed drop size distribution model. The coefficient a is further modified by the index of nonuniformity.

3. Attenuation correction

In this section, the attenuation correction method is described without taking into consideration the effect

of nonuniform distribution of rain within the radar resolution cell. The corrections needed for nonuniformity of rain are described in section 5. Given the assumption that the rain is uniform within the radar resolution cell, the observed radar reflectivity factor $Z_m(r)$ and the true effective radar reflectivity factor $Z_e(r)$ are related through

$$Z_m(r) = Z_e(r)A(r) = Z_e(r)\exp\left[-0.2\ln(10)\int_0^r k(s)\,ds\right], \quad (1)$$

where $A(r)$ is the attenuation factor from the radar to range r, and $k(r)$ is the specific attenuation or attenuation coefficient expressed in decibels per kilometer. Given an estimate of the attenuation factor $A(r)$, one can calculate $Z_e(r)$ from measured $Z_m(r)$ by $Z_e(r) = Z_m(r)/A(r)$.

If k is related to Z_e by a power law $k = \alpha Z_e^\beta$, then (1) can be solved for Z_e and the solution becomes

$$Z_e(r) = \frac{Z_m(r)}{A_{\rm HB}(r)}, \quad (2)$$

where $A_{\rm HB}(r)$ is given by

$$A_{\rm HB}(r) = \left[1 - q\beta\int_0^r \alpha(s)Z_m^\beta(s)\,ds\right]^{1/\beta}, \quad (3)$$

with $q = 0.2\ln(10)$ (Iguchi and Meneghini 1994). The solution (2) is equivalent to the Hitschfeld–Bordan solution for the attenuation correction (Hitschfeld and Bordan 1954).

Let PIA denote the two-way attenuation to the surface ($r = r_s$) expressed in units of decibels, that is,

$$\mathrm{PIA} = -10\log_{10}A(r_s) = -10\log_{10}\left[\frac{Z_m(r_s)}{Z_e(r_s)}\right]. \quad (4)$$

Then, the Hitschfeld–Bordan estimate of PIA becomes

$$\mathrm{PIA}_{\rm HB} = -10\log_{10}A_{\rm HB}(r_s) = -\frac{10}{\beta}\log_{10}(1-\zeta). \quad (5)$$

Here, ζ is defined as

$$\zeta = q\beta\int_0^{r_s}\alpha(s)Z_m^\beta(s)\,ds. \quad (6)$$

In many cases when rain is heavy, however, ζ exceeds unity and (5) becomes meaningless. Nevertheless, the quantity ζ can be used as a qualitative indicator of the magnitude of PIA from the rain echo.

The surface reference technique also gives an independent estimate of PIA (Meneghini et al. 2000). This PIA is denoted by $\mathrm{PIA}_{\rm SR}$. This technique assumes that the decrease of the apparent surface cross section is caused by the propagation loss of radar signal by rain:

$$\mathrm{PIA}_{\rm SR} = \Delta\sigma^0 = \langle\sigma^0_{\text{no-rain}}\rangle - \sigma^0_{\rm rain}. \quad (7)$$

In this equation, $\langle\sigma^0_{\text{no-rain}}\rangle$ indicates the average of the surface cross section in rain-free conditions for a given incidence angle. This decrease of the surface cross section is expressed in decibels and denoted by $\Delta\sigma^0$.

The objective here is to find the best estimate of PIA, denoted by PIA_e, from ζ and $\Delta\sigma^0$. Once the estimate of PIA_e is obtained, an attenuation correction factor ϵ is introduced in such a way that the modified Hitschfeld–Bordan estimate gives the same path attenuation as PIA_e:

$$\mathrm{PIA}_e = -\frac{10}{\beta}\log_{10}(1-\epsilon\zeta). \quad (8)$$

With this ϵ, the attenuation-corrected Z_e can be calculated at all ranges by (Iguchi and Meneghini 1994)

$$Z_e(r) = \frac{Z_m(r)}{\left[1 - \epsilon q\beta\int_0^r \alpha(s)Z_m^\beta(s)\,ds\right]^{1/\beta}}. \quad (9)$$

Because multiplying ζ by ϵ is equivalent to adjusting α, this is an α-adjustment method.

If the surface reference $\Delta\sigma^0$ is taken to be exact and if we set $\mathrm{PIA}_e = \mathrm{PIA}_{\rm SR} = \Delta\sigma^0$, the attenuation correction factor is given by

$$\epsilon = \epsilon_s = \frac{1 - 10^{\beta\Delta\sigma^0/10}}{\zeta}. \quad (10)$$

If we substitute this ϵ_s for ϵ in (9), we obtain the original α-adjustment solution of the surface reference method (Meneghini et al. 1983). If, on the other hand, the surface reference is totally ignored and the original ζ is taken to be exact, then $\mathrm{PIA}_e = \mathrm{PIA}_{\rm HB}$ and $\epsilon = 1$.

When the attenuation is small, the magnitude of $\Delta\sigma^0$ itself should be small. The measurement of the surface cross section, however, is always subject to measurement error, say e_{σ^0}. Unless $\Delta\sigma^0 \gg e_{\sigma^0}$, the use of the surface reference technique may be counterproductive, introducing larger errors in the estimate than if it were discarded entirely. On the other hand, when the attenuation is large, ζ becomes close to unity and the Hitschfeld–Bordan solution becomes unstable. In such a case, the relative error in $\mathrm{PIA}_{\rm SR}$ generally becomes small because $\Delta\sigma^0$ becomes large.

With such dependence of the attenuation estimate on ζ and $\Delta\sigma^0$ in mind, it is desirable to find a method that gives a reliable estimate of PIA_e from ζ and $\Delta\sigma^0$ or, equivalently, to find a weighting function that defines the value of ϵ between 1 and ϵ_s defined in (10). This is the idea of the hybrid method between the Hitschfeld–Bordan method and the surface reference method.

The approximate value of PIA can be judged from the magnitude of ζ because, if the rain is weak and its echoes at all ranges are small, ζ is naturally small. Because of this characteristic of ζ, the magnitude of ζ was used to define the weighting function between 1 and ϵ_s in an early version of the algorithm.

In version 5.53, however, an improved method is used. The problem can be stated in the following way. Given two independent quantities θ_1 and θ_2 that are both related to the PIA, find the most probable value of PIA.

In other words, find the PIA that maximizes the conditional probability for given θ_1 and θ_2:

$$p(\text{PIA}\,|\,\theta_1,\,\theta_2). \tag{11}$$

In the current case, θ_1 is a function of $\Delta\sigma^0$, and θ_2 is a function of ζ.

If a storm model is chosen, then we can calculate ζ and $\Delta\sigma^0$ from it. For example, once the vertical profile of α and the constant β are chosen, and if $Z_e(r)$ is given, one can calculate $Z_m(r)$ and hence ζ by using (6). In general, there are some uncertainties in α, β, and $Z_m(r)$ resulting from the unknown structure of the storm, the unknown drop size distribution, and signal fluctuations. Therefore, we can only specify the probability distribution of θ_2 for a given PIA:

$$p(\theta_2\,|\,\text{PIA}). \tag{12}$$

In a similar way, we can give the probability distribution of θ_1 for a given PIA:

$$p(\theta_1\,|\,\text{PIA}). \tag{13}$$

If it is assumed that θ_1 and θ_2 are independent parameters, (11) can be rewritten as follows by using Bayes's theorem:

$$p(\text{PIA}\,|\,\theta_1,\,\theta_2) = \frac{p(\theta_1\,|\,\text{PIA})p(\theta_2\,|\,\text{PIA})p(\text{PIA})}{\int p(\theta_1\,|\,\text{PIA})p(\theta_2\,|\,\text{PIA})p(\text{PIA})\,d\text{PIA}}. \tag{14}$$

If we assume our total ignorance of the PIA for each measurement, we may treat p(PIA) as a uniform distribution within a reasonably wide realistic range. Then $p(\text{PIA}\,|\,\theta_1,\,\theta_2)$ is proportional to $p(\theta_1\,|\,\text{PIA})p(\theta_2\,|\,\text{PIA})$. If both $p(\theta_1\,|\,\text{PIA})$ and $p(\theta_2\,|\,\text{PIA})$ are expressed in simple analytical forms, then the PIA that maximizes (14) can be calculated in a short time that is acceptable for operational data processing.

In the current case, we assume that the error in $\Delta\sigma^0$ is constant irrespective of the magnitude of $\Delta\sigma^0$ itself and is distributed normally around the mean. Then we set $\theta_1 = \Delta\sigma^0$ so that $p(\theta_1\,|\,\text{PIA})$ becomes

$$p(\theta_1\,|\,\text{PIA}) = \frac{1}{\sqrt{2\pi}\sigma_1}\exp\left\{-\frac{[\theta_1 - \theta_{10}(\text{PIA})]^2}{2\sigma_1^2}\right\} \tag{15}$$

with

$$\theta_{10}(\text{PIA}) = \text{PIA}. \tag{16}$$

Note that, with this formulation, $\Delta\sigma^0$ can take on negative values even if the true PIA is always positive. Negative values of $\Delta\sigma^0$ actually occur frequently when the attenuation is small.

If we can convert ζ into the same unit space as θ_1, the problem is simple, but, as seen from (5) and (6), we cannot, because ζ often exceeds 1 when attenuation is large. Because ζ takes only a positive value (because Z_m, α, and β are all positive) and because the major uncertainty in the model is the value of α (because fluctuations in Z_m caused by a finite number of sampling and noise should mostly cancel out when Z_m^β is summed over many range bins), we assume that the relative error in ζ is constant and that ζ is lognormally distributed for a given PIA. In other words, we assume

$$p(\theta_2\,|\,\text{PIA}) = \frac{1}{\sqrt{2\pi}\sigma_2}\exp\left\{-\frac{[\theta_2 - \theta_{20}(\text{PIA})]^2}{2\sigma_2^2}\right\} \tag{17}$$

with

$$\theta_2 = \ln(\zeta) \quad \text{and} \tag{18}$$

$$\theta_{20}(\text{PIA}) = \ln\{1 - \exp[-0.1\beta\ln(10)\text{PIA}]\}. \tag{19}$$

From (15) and (17),

$$\begin{aligned} p(\text{PIA}\,|\,\theta_1,\,\theta_2) &\propto \frac{1}{\sqrt{2\pi}\sigma_1}\exp\left[-\frac{(\theta_1 - \theta_{10})^2}{2\sigma_1^2}\right]\frac{1}{\sqrt{2\pi}\sigma_2} \\ &\quad\times \exp\left[-\frac{(\theta_2 - \theta_{20})^2}{2\sigma_2^2}\right] \\ &= \frac{1}{2\pi\sigma_1\sigma_2}\exp\left\{-\left[\frac{(\theta_1 - \theta_{10})^2}{2\sigma_1^2} + \frac{(\theta_2 - \theta_{20})^2}{2\sigma_2^2}\right]\right\}. \end{aligned} \tag{20}$$

The PIA that maximizes $p(\text{PIA}\,|\,\theta_1,\,\theta_2)$ is the same as the PIA that minimizes distance d that is defined by

$$d^2 = \frac{(\theta_1 - \theta_{10})^2}{2\sigma_1^2} + \frac{(\theta_2 - \theta_{20})^2}{2\sigma_2^2}. \tag{21}$$

Because θ_{10} and θ_{20} are related through (16) and (19), if we take θ_{10}/σ_1 and θ_{20}/σ_2 as x and y in a rectangular coordinate system and draw a curve defined by (16) and (19), then the solution that minimizes (21) can be found as the nearest point on the curve from the point given by the measured pair of $(\theta_1/\sigma_1,\,\theta_2/\sigma_2)$. See Fig. 2.

In version 5.53 of 2A25, σ_2 is assumed to be 1 dB, whereas σ_1 is taken from 2A21, which gives $\Delta\sigma^0$ and the magnitude of fluctuation in σ^0. However, to avoid erroneous dependence on the surface reference, the standard deviation of σ^0 from 2A21 is used as σ_1 only when it is larger than a threshold value. In other words, we assume a minimum error in the surface cross-section stability and measurement. This minimum error is assumed to be 1 dB over ocean and 3 dB over land. The final error in the estimate of the total path attenuation is calculated as the standard deviation of (20).

If $\Delta\sigma^0$ is not available from 2A21 or not reliable, we calculate the equivalent attenuation $\Delta\sigma_c^0$ that would result if the true Z_e profile were constant near the surface and if the apparent decrease of Z_m with range there were caused entirely by rain attenuation. In other words, $\Delta\sigma_c^0$ is the attenuation that would make the attenuation-corrected Z_e profile constant near the surface if it were used in the surface reference method with $\epsilon = \epsilon_s$. In the actual algorithm, $\Delta\sigma_c^0$ is substituted for $\Delta\sigma^0$, and the best ϵ is sought by the minimization program mentioned above. Because the minimization routine gives a

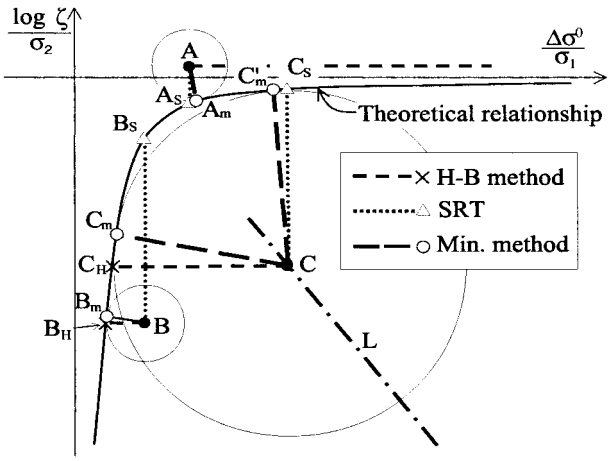

FIG. 2. Diagram for finding the most likely path-integrated attenuation from a given pair of $\Delta\sigma^0$ and ζ. Points A, B, and C represent measured pairs of $(\Delta\sigma^0/\sigma_1, \log\zeta/\sigma_2)$. The theoretical curve is given by (16) and (19). Here B_H and C_H are the intersections of the theoretical curve and the horizontal lines through the data points (B, C), and they correspond to the Hitschfeld–Bordan solutions. Note that when $\zeta \geq 1$ (case A), there is no Hitschfeld–Bordan solution (A_H). The points A_S, B_S, and C_S are the intersections of the theoretical curve and the vertical lines through A, B, and C, respectively, and they correspond to the solutions with the surface reference technique (SRT). The maximum likelihood solutions for these given data points are the nearest points on the theoretical curve from the data points and are shown by A_m, B_m, C_m, and C'_m. Note that when the data point is on half-line L, there are two solutions. We take C_m in such a case, as explained in the text.

value of ϵ between 1 and ϵ_s, the use of this constant-Z_e-near-the-surface assumption does not necessarily give a constant Z_e near the surface. In fact, when $\Delta\sigma^0$ is not reliable because of small attenuation, ϵ becomes close to 1, and the final profile is nearly independent of $\Delta\sigma_c^0$. If the measured reflectivity profile actually increases as the surface is approached, $\Delta\sigma_c^0$ is set to 0. This assumption of constant Z_e near the surface may not be a scientifically justifiable assumption, but is adopted on a ''better-than-nothing'' basis (Marzoug and Amayenc 1994). In fact, it not only prevents the Hitschfeld–Bordan solution from unstable divergence, it often gives reasonable profiles (Amayenc et al. 1996).

As mentioned above, the attenuation correction method described in this section works for all positive and negative values of $\Delta\sigma^0$ and $\log\zeta$, in principle. However, if ζ is very small, we can safely conclude that there is little rain. In such a case, it is better to ignore the surface reference data entirely to avoid contamination by outliers in surface reference data. In fact, $\Delta\sigma^0$ occasionally takes an unrealistically large value, particularly over land, when the reference surface includes a surface or object with extremely large scattering cross section or when the surface under rain is not properly identified. In the current algorithm, if ζ is less than 0.2, then $\Delta\sigma^0$ is reset to 0.5 dB before it is handed to the minimization routine. A PIA of 0.5 dB approximately corresponds to $\zeta = 0.1$, which is the average of ζ in the domain for this exceptional processing. The actual value to which $\Delta\sigma^0$ is set in this domain is not very important as long as $\Delta\sigma^0$ is kept reasonably small, because the solution of the minimization is essentially the same as that of the Hitschfeld–Bordan solution in this domain. Insensitivity of the solution to $\Delta\sigma^0$ comes from the large slope in Fig. 2 for small ζ. By limiting the domain of ζ for which the original $\Delta\sigma^0$ is used in the minimization algorithm, we can also avoid nonuniqueness of the minimization problem in an unusual situation. In fact, in the region defined by very small ζ and very large $\Delta\sigma^0$, there are points from which we can draw a circle that is tangent to the solution curve at two points if the distance from the data point to the solution curve in Fig. 2 is larger than the minimum radius of curvature of the theoretical curve. In such a contradictory region—contradictory because a small ζ implies small attenuation whereas a large $\Delta\sigma^0$ implies large attenuation—it is generally true that $\Delta\sigma^0$ is in error and that ζ is the more reliable measure of attenuation.

Although the weighting function is not explicitly used in the attenuation correction method explained here, it is essentially the same as the hybrid method described in Iguchi and Meneghini (1994). The equivalent weight is now determined not only by the value of ζ as suggested there, but also by the surface reference $\Delta\sigma^0$. In the earlier version of 2A25, only two weighting functions were used. The function forms were also somewhat artificial, that is, linear and quadratic functions. One of them was selected according to the reliability of $\Delta\sigma^0$ from 2A21. In the new method, however, the error estimates in ζ and $\Delta\sigma^0$ are treated as continuous parameters in the definition of the weighting function. The old and new methods give nearly the same ϵ when both ζ and $\Delta\sigma^0$ are large. However, when they are not large, substantial difference can be seen. In the previous versions, the *Z–R* relation was not adjusted even though the *k–Z* relation was adjusted by the surface reference through the α-adjustment method. In such an algorithm, the actual estimate of ϵ for small ζ is not very important because the attenuation correction remains small ($Z_e \approx Z_m$) and the rain estimates are not affected by ϵ. In the new version of the algorithm, however, the *Z–R* relation is adjusted in accordance with the adjustment in *k–Z* relation to be consistent with the drop size distribution (DSD) model assumed. As a result, the accuracy of the estimate in ϵ is equally important for small ζ as well as large ζ. Therefore, the weighting function must be carefully determined for all ranges of ζ. The new algorithm described here gives a possible solution to defining such a weighting function.

Figure 3 shows a scatterplot of $\Delta\sigma^0$ and $10\log_{10}(\zeta)$ from one orbit of PR data (orbit 644, 7 January 1998) together with the model curve. Note that the weighted distance [(21)] used in the minimization is not the same as the apparent distance from each data point to the curve in this figure, because the weighted distance depends on the standard deviations σ_1 and σ_2. The distribution of data points around the model curve and the histogram of ϵ (see Fig. 5, described in section 6) in-

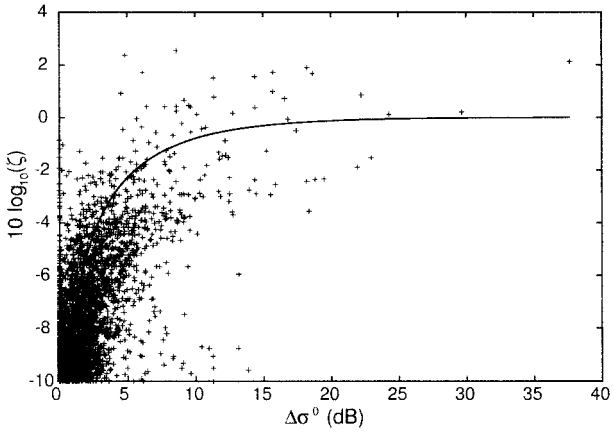

FIG. 3. The scatterplot of $\Delta\sigma^0$ and 10 $\log_{10}(\zeta)$ from one orbit of PR data. The solid line indicates the model. Note that the weighted distance [(21)] used in the minimization is not the same as the apparent distance from each data point to the curve in this figure, because the weighted distance depends on the standard deviations σ_1 and σ_2.

dicate that the normality assumption of the distribution of $\ln(\zeta)$ for a given PIA is reasonable.

If the measured Z_m is biased by a constant factor, data points in a scatterplot such as Fig. 3 shift vertically parallel to the ordinate. The optimum solution changes accordingly. However, when the PIA to the surface is very small or very large and if the data point is not very far from the model curve, the estimated PIA from the solution, which corresponds to the horizontal coordinate of the solution on the model curve, remains nearly the same for a small vertical shift of the data point. This result occurs either because the model curve has a steep slope in the region of small PIA so that a vertical shift along the solution curve has little effect on the horizontal coordinate or because the model curve has a shallow slope in the region of large $\Delta\sigma^0$ so that a vertical shift of the data point has a negligible effect on the solution. In these regions, because the attenuation correction is virtually unchanged, the denominator in the right-hand side of (9) remains nearly the same, and the bias in Z_m is translated almost directly into the attenuation-corrected Z_e. This is a graphical explanation of the fact that when the PIA is very small the attenuation correction itself is negligible, and when the PIA is very large the attenuation correction is determined not by the rain echo but by the surface reference, which is free from bias error. In the intermediate attenuation range, however, a positive bias in Z_m moves the solution toward the upper right of the model curve in Fig. 2 and increases the amount of attenuation correction. As a result, the final Z_e increases more than the bias in Z_m. The magnitude of the extra correction resulting from the bias in Z_m depends on ζ, $\Delta\sigma^0$, and their error estimates but never exceeds $(\sigma_1/2\sigma_2)\Delta\text{dB}Z_m$, where $\Delta\text{dB}Z_m$ is the bias in Z_m (dBZ).

4. DSD model

In the conversions from Z_m to attenuation-corrected Z_e, and from Z_e to R, we need to assume k–Z_e and Z_e–R relations, or, equivalently, a DSD. The appropriate selection of the DSD model is very important because it will affect the final estimates of R substantially. In version 5.53 of 2A25, both k–Z_e and Z_e–R relations are adjusted in accordance with the assumed DSD model (Kozu et al. 1999). We assume two DSD models corresponding to stratiform and convective rain. The models were made from a collection of Z–R relations measured near the ocean from widely distributed locations around the world (Ajayi and Owalabi 1987; Austin and Geotis 1979; Cunning and Sax 1977; Short et al. 1990; Stout and Mueller 1968; Tokay and Short 1996). For each model, we convert the observed Z–R relationship into an N_0–Λ relationship, where N_0 and Λ are parameters in the size distribution:

$$N(D) = N_0 D^{\mu} \exp(-\Lambda D). \tag{22}$$

Here, D is drop diameter. We assume that μ is constant and takes a value of $\mu = 3$. The selection of the value of μ is not very important because the final k–Z_e and Z_e–R relations derived are nearly the same, even though different values of μ would give seemingly different relations between N_0 and Λ (Kozu et al. 1999).

Once the DSD model is thus selected, the corresponding k–Z_e and Z_e–R relations at the PR frequency of 13.8 GHz can be calculated for rain and snow at different temperatures and mixing ratios. The initial values of these coefficients for different rain types are calculated in the following way.

For stratiform rain with a bright band, we use the stratiform DSD model with a vertical profile model by Nishitsuji (Awaka et al. 1985). This brightband model is a nonbreakup noncoalescence model and is known to explain the propagation characteristics at 34.5 GHz and 11.5 GHz in the *Japanese Experimental Telecommunication Satellite-II* (Nishitsuji et al. 1983). The coefficients in the k–Z_e and Z_e–R relations are calculated for snow–water mixtures with fractional water contents of 17%, 1.7%, and 1.1%. The coefficients are also computed for water drops at temperatures of 20° and 0°C. The coefficients for a snow–water mixture of 17% water are used at the brightband peak; those at 1.7% water are used at 500 m above the bright band; and those at 1.1% water are used at the storm top. For distances greater than 500 m below the brightband peak, the hydrometeors are assumed to be fully melted. The k–Z_e and Z_e–R coefficients at intermediate levels are calculated by linear interpolation. The coefficients at heights above the surface and 500 m below the bright band are calculated from the temperature assuming a lapse rate of 5°C km^{-1}, where the 0°C level is assumed to occur at a height 500 m below the brightband peak. After the temperature is calculated, the coefficients are found by a linear interpolation or extrapolation of the results at 0° and 20°C. See Fig. 4.

For stratiform rain in the absence of a detectable bright

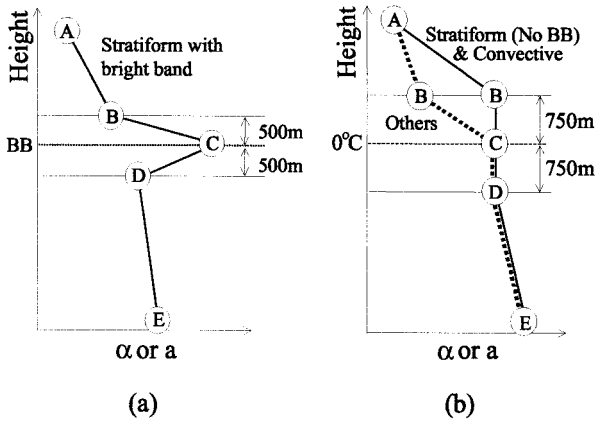

FIG. 4. Schematic presentation of the profiles of α and a. The initial values of a, b, and α are given at five points, A, B, C, D, and E. When a bright band is detected (a), C is chosen at the brightband (BB) center, B is two range bins above C, D is two range bins below C, A is the top of the echo, and E is the lowest valid range bin. If there is no bright band (b), C is chosen at the estimated freezing height, and B and D are 750 m above and below C, respectively. Here A and E are the same as before. Coefficients between these points are calculated by interpolation. Note that the profile for stratiform rain without a bright band is similar to that for convective rain, but their actual values are different.

band, the stratiform DSD model is again used but with the hydrometeors assumed to be at 0°C in the interval ±750 m on either side of the 0°C isotherm. In this case, the 0°C isotherm is estimated using the climatological surface temperature and a lapse rate of 5°C km^{-1}.

For convective rain, the convective DSD model is used. The vertical profile assumed is exactly the same as that for stratiform rain without a bright band.

For rain categorized as ''others'' by 2A23, the model used is almost the same as that for convective rain, but the 0°C water phase is assumed only up to the 0°C height, and the coefficients for a 1.7% mixture are used at 750 m above the 0°C height. This choice of profile is based on the observation that rain categorized as others is generally weak, isolated rain and is unlikely to have extended water phase well above the 0°C isotherm. Actual values used in version 5.53 of 2A25 are listed in Table 1. The coefficients at point E in Fig. 4 are calculated by interpolation or extrapolation of the coefficients at 0°C and 20°C.

As noted in section 3, the initial values of a and b are adjusted in accordance with the change in α in $k = \alpha Z_e^{\beta}$ in the process of attenuation correction. The new a and b coefficients in $R = \alpha Z_e^{\beta}$ are calculated in such a way that the adjusted pair (a, b) is consistent with the pair (α, β) when they are both converted into the relation between N_0 and Λ of the DSD model. In the actual program, the correction factors for a and b are expressed as quadratic functions of ϵ. Unlike the k–Z_e relation, the Z_e–R relation depends on the air density, and therefore height, a consequence of the fact that the rain rate is a function of the raindrop fall speeds, which, in turn, are determined by raindrop sizes and air density (Foote and du Toit 1969). The coefficient a is further multiplied by the nonuniform beam-filling (NUBF) correction factor for the Z_e–R relationship to compensate for the nonuniform rain distribution within the resolution cell.

When attenuation is large, the weight in the hybrid method is shifted toward the surface reference, and the final PIA is virtually determined by $\Delta\sigma^0$. In such cases, the initial value of α in the model has little effect on the final Z_e near the surface, because it is essentially determined by the measured Z_m and the PIA at the surface. As a result, the coefficients a and b are only weakly dependent on the initial values. When attenuation is small or marginal, however, the surface reference constraint perturbs the initial choices of a and b only slightly. Therefore, an appropriate selection of the initial DSD model is very important for relatively weak rain.

TABLE 1. Initial k–Z_e and Z_e–R parameters ($k = \alpha Z_e^{\beta}$, $R = aZ_e^{b}$, $Z_e = a''R^{b''}$).

		Position shown in Fig. 4				
Parameter		A	B	C	D (0°C water)	20°C water
Stratiform	α	0.000 086 1	0.000 108 4	0.000 414 2	0.000 282 2	0.000 285 1
	β	0.792 30	0.792 30	0.792 30	0.792 30	0.792 30
	a	0.013 98	0.012 63	0.004 521	0.020 10	0.022 82
	b	0.7729	0.7644	0.7288	0.6917	0.6727
	a''	250.8	304.6	1649.3	283.9	275.7
	b''	1.294	1.308	1.372	1.446	1.487
Convective	α	0.000 127 3	0.000 410 9	0.000 410 9	0.000 410 9	0.000 417 2
	β	0.7713	0.7713	0.7713	0.7713	0.7713
	a	0.020 27	0.034 84	0.034 84	0.034 84	0.040 24
	b	0.7556	0.6619	0.6619	0.6619	0.6434
	a''	174.1	159.5	159.5	159.5	147.5
	b''	1.323	1.511	1.511	1.511	1.554
Others	α	0.000 127 3	0.000 159 8	0.000 410 9	0.000 410 9	0.000 417 2
	β	0.7713	0.7713	0.7713	0.7713	0.7713
	a	0.020 27	0.018 71	0.034 84	0.034 84	0.040 24
	b	0.7556	0.7458	0.6619	0.6619	0.6434
	a''	174.1	207.4	159.5	159.5	147.5
	b''	1.323	1.341	1.511	1.511	1.554

5. Nonuniform beam-filling corrections

The treatment of the attenuation in radar echoes through rain in the previous sections assumes that the rain is horizontally uniform within the radar beam, that is, in the plane orthogonal to the direction of electromagnetic propagation. Because the footprint size of the PR is about 4.3 km at nadir, however, uniformity of rain within the radar beam is not guaranteed. If rain is nonuniform within the beam, both the k–Z_e and Z_e–R relations for uniform rain must be modified, because these relations are nonlinear.

Let a vector $\mathbf{x}$ represent a position in a plane perpendicular to r. We assume that R is a function of both r and $\mathbf{x}$. We also assume that we know the coefficients a and b applicable at each point: $R(r, \mathbf{x}) = aZ_e^b(r, \mathbf{x})$. If the attenuation effect is excluded, the measured radar reflectivity factor is the average of $Z_e(r, \mathbf{x})$ over a radar resolution cell which is centered at r_0 and $\mathbf{x}_0$:

$$Z_{\text{obs}}(r_0, \mathbf{x}_0) = \langle Z_e \rangle = \iint G(r, \mathbf{x}) Z_e(r_0 + r, \mathbf{x}_0 + \mathbf{x})\, dr\, d\mathbf{x}, \quad (23)$$

where $G(r, \mathbf{x})$ is a weighting function whose integral is normalized to unity. Function $G(r, \mathbf{x})$ is determined by the pulse shape and the antenna pattern. We can similarly define the average rainfall rate within the radar resolution cell centered at r_0 and $\mathbf{x}_0$:

$$\langle R \rangle = \iint G(r, \mathbf{x}) R(r_0 + r, \mathbf{x}_0 + \mathbf{x})\, dr\, d\mathbf{x}. \quad (24)$$

Because b is less than unity and aZ_e^b is a concave function, it can be shown by using Jensen's equality (Hardy et al. 1952) that

$$\langle R \rangle = \langle aZ_e^b \rangle \le a \langle Z_e \rangle^b. \quad (25)$$

To estimate $\langle R \rangle$ from measured $\langle Z_e \rangle$, we need to find a' and b' that satisfy the relation

$$\langle R \rangle = a' \langle Z_e \rangle^{b'} \quad (26)$$

from the original a and b and nonuniformity information. We characterize the nonuniformity of rain by the probability distribution of k. If this probability distribution is a lognormal or gamma distribution, it can be shown that

$$b' = b \quad \text{and} \quad a' = aC_{ZR}, \quad (27)$$

where C_{ZR} is the correction factor for the Z_e–R relation. This correction factor depends only on the normalized standard deviation σ_n of k within the scattering volume and is independent of k or Z_e itself. The details are described in the appendix.

In a similar way, $\langle k \rangle$ is less than $\alpha \langle Z_e \rangle^\beta$. The effect of nonuniformity of rain for the attenuation correction is more complicated than that for the Z_e–R relation, however, because the attenuation is a path-integrated quantity. If the ray approximation is valid, the attenuation factor at r is

$$A(r, \mathbf{x}) = \exp\left[-0.2 \ln(10) \int_0^r k(s, \mathbf{x})\, ds\right]. \quad (28)$$

If this attenation factor is averaged over horizontal directions, it will become

$$\langle A(r, \mathbf{x}) \rangle = \int G(\mathbf{x}) \exp\left[-0.2 \ln(10) \int_0^r k(s, \mathbf{x})\, ds\right] d\mathbf{x}, \quad (29)$$

where $G(\mathbf{x})$ is the weighting function whose integral is normalized to unity and represents the two-way antenna pattern. The attenuation estimate from the surface reference technique corresponds to this quantity. This attenuation factor is different from the attenuation factor calculated from the horizontally averaged attenuation coefficient:

$$\exp\left[-0.2 \ln(10) \int_0^r \int G(\mathbf{x}) k(s, \mathbf{x})\, d\mathbf{x}\, ds\right]. \quad (30)$$

Furthermore, even if rain is vertically uniform and $k(r, \mathbf{x})$ is independent of r, the apparent specific attenuation cannot be expressed by a range-independent constant. In other words, if $k(\mathbf{x})$ is a function of $\mathbf{x}$, it is not possible to find a constant k' that satisfies the following equation:

$$\int G(\mathbf{x}) \exp[-0.2 \ln(10) k(\mathbf{x}) r]\, d\mathbf{x} = \exp[-0.2 \ln(10) k' r]. \quad (31)$$

This fact can be easily understood if one imagines a case in which two shafts of rain with different intensities fill each half of a vertically directed beam. Let one half of the beam be filled by rain with radar reflectivity factor of Z_1 and the other half by rain with Z_2. Then, the measured radar reflectivity factor becomes

$$Z_m(r) = \frac{Z_1}{2} \exp[-0.2 \ln(10) k_1 r] + \frac{Z_2}{2} \exp[-0.2 \ln(10) k_2 r]. \quad (32)$$

Here, k_1 and k_2 are specific attenuations for the two rain regions. Range r is assumed to be measured downward from the rain top and the rain is assumed to be vertically uniform below the rain top to the surface. If $Z_1 \gg Z_2$, then $Z_m(r)$ varies like $(Z_1/2) \exp[-0.2 \ln(10) k_1 r]$ for small r. This relation means the apparent specific attenuation is close to k_1. For large r, however, the first term on the right-hand side becomes smaller than the second term because $k_1 \gg k_2$. As a result, only the echo from the less attenuated half remains, and the signal decreases with distance with a specific attenuation close to k_2. In this example, the average radar reflectivity factor $\langle Z_e \rangle$ at each range is $(Z_1 + Z_2)/2$ and is constant, but the apparent attenuation coefficient changes with r. This fact implies that the specific attenuation we need for the attenuation correction cannot

be calculated only from the average $\langle Z_e \rangle$ and the local nonuniformity. We need to know the horizontal structure of rain at all ranges.

This observation exemplifies the difficulty of attenuation correction at all ranges if rain is not uniform. In fact, unless we know the detailed structure of rain distribution, it is impossible to correct for the attenuation. Because we can obtain only the averaged radar reflectivity factor $\langle Z_m \rangle$, we need to be satisfied with a method that, at best, gives statistically unbiased attenuation estimates. In version 5.53 of 2A25, only the nonuniform effect on the total path attenuation is considered. No correction is attempted for a range-dependent correction, and the change in nonuniformity along the range direction is effectively neglected.

If some nonuniformity in the rain distribution is present in the horizontal direction, the path-integrated attenuation to the surface is

$$\mathrm{PIA}_{\mathrm{NU}} = -10 \log_{10} \langle A(r_s, \mathbf{x}) \rangle = -10 \log_{10} \left\{ \int G(\mathbf{x}) \exp\left[-0.2 \ln(10) \int_0^{r_s} k(s, \mathbf{x})\, ds \right] d\mathbf{x} \right\}. \quad (33)$$

On the other hand, what we want is the path-integrated attenuation that would result if the same amount of rain in the radar beam were to be distributed uniformly over the radar beam. Let this attenuation be denoted by PIA_u, then

$$\mathrm{PIA}_u = -10 \log_{10} \exp\left[-0.2 \ln(10) \int_0^{r_s} \alpha \langle Z_e(s) \rangle^{\beta}\, ds \right]. \quad (34)$$

If we use PIA_u instead of $\mathrm{PIA}_{\mathrm{NU}}$ as the path attenuation from the surface reference technique, then the attenuation-corrected $Z_e(r)$ would be consistent with the total path attenuation that is caused by the averaged $\langle Z_e \rangle$ at each range, even though the correction at each range may not be correct.

To estimate the path attenuation PIA_u for uniform rain, we assume that it can be estimated from the estimated $\mathrm{PIA}_{\mathrm{NU}}$ for nonuniform rain and its normalized standard deviation within the radar beam. Let PIA at $\mathbf{x}$ within the beam be denoted by $\mathrm{PIA}(\mathbf{x})$, its mean by m_{PIA}, and its standard deviation by σ_{PIA}. The normalized standard deviation σ_n of PIA within the radar beam is then defined by

$$\sigma_n = \frac{\sigma_{\mathrm{PIA}}}{m_{\mathrm{PIA}}}. \quad (35)$$

We assume that $\mathrm{PIA}(\mathbf{x})$ is lognormally distributed. Then, we can calculate $\mathrm{PIA}_{\mathrm{NU}}$ numerically for a given m_{PIA} and σ_n. By inverting this relation and with the assumption of the lognormality of PIA distribution, we can calculate PIA_u from $\mathrm{PIA}_{\mathrm{NU}}$ and σ_n. Details are explained in the appendix. $\mathrm{PIA}_{\mathrm{NU}}$ can be approximately estimated from the measured surface reference $\Delta\sigma^0$ and radar echoes by using the method described in section 3. Because σ_n is not a measurable quantity, we estimate it from a normalized standard deviation of PIAs estimated in coarse resolutions. Actually, the normalized standard deviation of the nine PIAs in 3×3 radar beams with the beam in question at the center is used for this purpose. The relations between the normalized standard deviation in the coarse resolution and that in the fine resolution for different rain types are estimated from horizontal rain structures observed by a shipborne radar during the Tropical Ocean and Global Atmosphere Coupled Ocean–Atmosphere Research Experiment (Kozu and Iguchi 1999).

As described in section 2, the hybrid method is used twice. In the first instance, the $\mathrm{PIA}_{\mathrm{NU}}$ for each beam is estimated by retrieving the Z_e profile without taking the NUBF effect in the surface reference into account. The $\mathrm{PIA}_{\mathrm{NU}}$ estimates thus obtained are used to calculate the NUBF correction factors for the surface reference (C_{SR}) and the Z_e–R relation (C_{ZR}). The surface reference $\Delta\sigma^0$ is then modified by C_{SR}. The hybrid method is applied with this modified surface reference in the second instance, and the attenuation-corrected Z_e profile is calculated.

The nonuniform beam-filling effect of rain on the Z_e–R relation is generally small—in most cases less than 5%. The maximum correction is limited to 20% in 2A25, that is, $C_{ZR} \geq 0.8$. On the other hand, the NUBF correction for PIA depends on both σ_n and PIA. As a result, it is small when PIA is small. When PIA is large, however, it may become very large. To avoid an erroneously large adjustment, the maximum of C_{SR} is limited to 1.3. Note that C_{SR} is a multiplicative factor of PIA expressed in decibel units. If the PIA is 20 dB, for example, the correction can be as large as 6 dB for a total PIA of 26 dB. The NUBF correction for PIA becomes significant only in the vicinity of very strong convective rain shafts, whereas the NUBF correction for the Z_e–R relation becomes relatively large near the storm edges as well. Because the index of nonuniformity is estimated in a conservative way, C_{SR} rarely exceeds the artificial upper bound of 1.3.

6. Discussion

Among the three critical steps of the algorithm described in the previous sections, the most important step is the attenuation correction because it can change the

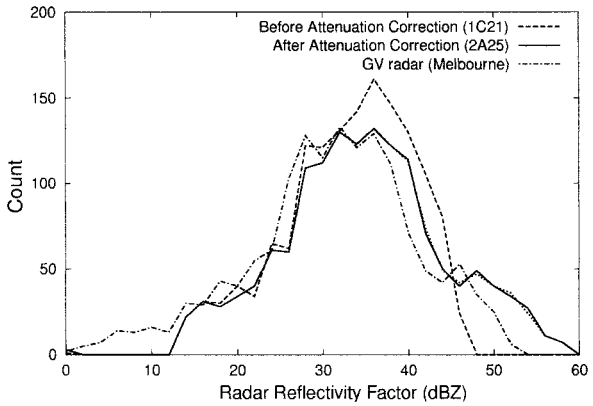

FIG. 5. Histograms of measured dBZ_m (dashed line) and attenuation-corrected dBZ (solid line) from the TRMM PR, and that of dBZ (dot–dashed line) nearly simultaneously measured by the WSR-88 radar in Melbourne, Florida, at 3 km above sea level in an overlapping area. The dotted line that almost overlaps the solid line denotes the histogram of attenuation-corrected dBZ without the nonuniform beam-filling correction. Note that the difference between the attenuation-corrected dBZ from the TRMM PR and the WSR-88 measurements can be explained by the fact that the effective radar reflectivity factor at 13.8 GHz is higher than the true radar reflectivity factor at a high-reflectivity range.

radar reflectivity factor by a factor of 10 or more if the attenuation is significant. The assumed DSD and the nonuniform beam-filling correction also affect the amount of the attenuation correction, but by an amount much smaller than the attenuation correction itself.

Figure 5 shows histograms of measured dBZ_m (dashed line) and attenuation-corrected dBZ (solid line) from version-5 TRMM PR products (orbit 1600, 9 March 1998), and that of dBZ (dot–dashed line) nearly simultaneously measured by the Weather Surveillance Radar-1988 Doppler (WSR-88D) in Melbourne, Florida, at 3 km above sea level in an overlapping area. The attenuation-corrected dBZ from the PR and WSR-88D measurements show similar distributions. Higher-dBZ values from the PR than the corresponding values from the WSR-88D measurements can be explained mostly by the difference between the effective dBZ_e at 13.8 GHz and that in the C band. A simulation from measured DSDs indicates that the difference in dBZ_e between these bands becomes significant above 30 dBZ and increases to 2–3 dB in the 40–50 dBZ range on average. The actual difference depends on DSD. The dotted line that almost overlaps the solid line denotes the histogram of attenuation-corrected dBZ without the nonuniform beam-filling correction. Because the parameters for the nonuniform beam-filling correction for attenuation are selected in a conservative way, the statistical distributions of dBZ with and without the NUBF correction are nearly the same in this version.

The example above and other processed data from the early phase of the mission prove that the attenuation correction with the proposed hybrid method works well. For the attenuation correction, the earlier versions of 2A25 and the new version give approximately the same results statistically. Both the attenuation-corrected reflectivity factors and the rain estimates from the earlier versions are within reasonable bounds (Kummerow et al. 2000).

However, a closer look at the early comparisons of the rain estimates with those by other means indicated that the 2A25 rain estimates were lower than other estimates in most cases. Such comparisons include the comparisons with a monthly zonal average over the ocean estimated from TRMM microwave imager data, instantaneous area averages of the Automated Meteorological Data Acquisition System rain gauge data, time-averaged rainfall rates estimated from disdrometer data at Nagoya University, and monthly regional rain accumulations from rain gauge data in India.

The disagreement with other estimates did not necessarily imply that the PR estimates were wrong. Nevertheless, there was some room for adjustment in the early version of the algorithm. One of the problems was that, although the surface reference method adjusted the coefficient of the k–Z_e relation, the corresponding Z_e–R relation was not adjusted. Because the k–R relation is more stable than the k–Z_e or Z_e–R relations in general, adjustment of the k–Z_e relation without a corresponding adjustment of the Z_e–R relation is equivalent to assuming a very unrealistic change in DSD. It was desirable to adjust the Z_e–R relation simultaneously with the k–Z_e relation in a consistent way. To realize such an adjustment, a new algorithm to estimate ϵ was needed, and the new method described in this paper was developed.

To select an appropriate DSD model, we took statistics of ϵ for large attenuation cases in convective storms. Because ϵ is in a sense the ratio of the attenuation estimate from the surface reference to that from the assumed k–Z_e relation, if the assumed DSD model is unbiased, it should be distributed around 1. We chose a global DSD model that was derived from the average of several known Z–R relations widely distributed over the TRMM coverage area. When compared with a DSD model based on data from Kapingamarangi Atoll, the global model gives a mean ϵ closer to unity for rain over the ocean.

The same method does not work well for the selection of a DSD model for stratiform rain, because stratiform rain is generally weak. In a weak PIA case, ϵ is always close to 1 because of the large slope of the model curve in Fig. 2, and different DSD models that shift the data points vertically in the plot do not alter the ϵ statistics very much. We therefore chose the stratiform Z_e–R model associated with the chosen convective model.

One important aspect of the ϵ statistics is the fact that the mean ϵ over land is much lower than unity if the global DSD or Kapingamarangi DSD model is used. Figure 6 shows the histograms of ϵ over the ocean and land for the global DSD model. The fact that ϵ is generally smaller than unity over land implies that the attenuation estimate from the radar echo using the assumed k–Z_e relation tends to be larger than the attenuation estimate from the surface reference. This bias in

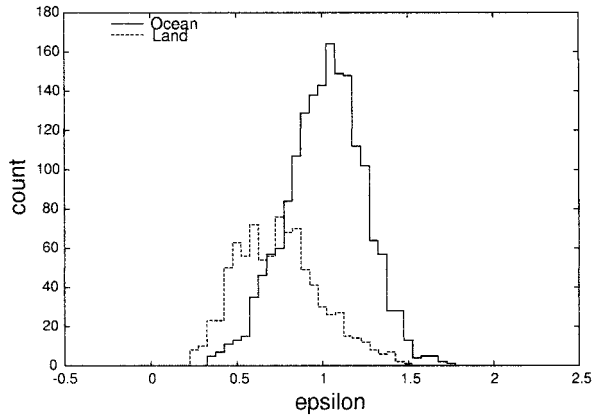

FIG. 6. Typical histograms of ϵ for convective rain over ocean and land. The histograms are taken from all angle bin data in which the final estimate of the path-integrated attenuation is larger than 10 dB. The solid line indicates the histogram for data over ocean, and the broken line is for data over land. The data used are 32 granules from 1–2 Jun 1998 (granules 3298–3329).

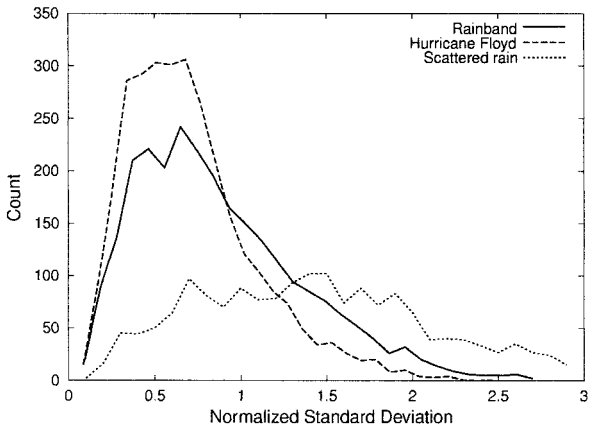

FIG. 7. Histograms of normalized standard deviation σ_n from three different heavy rain systems in orbit 4283 (26 Aug 1998). Each histogram is made from 150 successive scans of measurements that correspond to an observation area of approximately 220 km $\times$ 650 km. The three systems are a rainband in the eastern Pacific (solid line), Hurricane Floyd in the western Atlantic (broken line), and scattered rain (dotted line) in Africa.

ϵ in large attenuation cases does not originate in the bias of the surface reference, but in the assumed DSD model or the vertical structure of storms, because ζ itself tends to exceed unity over land when rain is heavy.

If this difference in statistics between the ocean and land is caused by the difference in DSD, the result implies that there are relatively more large rain drops and fewer small drops over land than over ocean for the same rainfall rate. However, the possibility that the difference is caused by an inappropriate vertical structure model cannot be ruled out. For example, water-phase hydrometeors are assumed to exist up to 750 m above the estimated freezing height. If the actual water-phase region ends at a much lower height than the assumed freezing height and if there is a high-reflectivity region above this level caused by ice-phase particles, then the actual attenuation may be much lower than the attenuation calculated with the assumption of water phase around the freezing height. In such a case, ζ may exceed unity.

Another possibility is a strong nonuniformity of rain. As discussed in the previous section, the actual attenuation in a nonuniform storm is always smaller than that calculated from the average $\langle Z_e \rangle$. Therefore, ζ may exceeds unity if rain is heavy and the nonuniformity is large, even when the assumed k–Z_e coefficients are locally appropriate. Figure 7 shows typical histograms of the normalized standard deviation (NSD) from three different heavy rain systems in orbit 4283 (26 August 1998). Each histogram is made from 150 successive scans of measurements that correspond to an observation area of approximately 220 km $\times$ 650 km. The three systems are a rainband in the eastern Pacific (solid line), Hurricane Floyd in the western Atlantic (broken line), and scattered rain (dotted line) in Africa. It can be seen from this figure that the statistical distribution of NSD depends on the rain system.

Although at present we do not have sufficient truth data to isolate the cause of the small ϵ over land, it can be safely said that the statistics of ϵ clearly indicate that rain over land has different characteristics from rain over ocean.

7. Conclusions

The rain-profiling algorithm for the TRMM precipitation radar is described. To estimate rainfall rate without bias, it is necessary to know the appropriate k–Z_e and Z_e–R relations. This necessity is a fundamental difficulty in radar meteorology. The TRMM PR data are also subject to this difficulty. However, part of this difficulty is alleviated by taking advantage of the peculiarity of the spaceborne radar, that is, the surface echo. The use of the surface reference method enables us to narrow the possible range of the raindrop size distribution. In fact, the hybrid method proposed in this paper appears to work very well. However, the nonuniform rain distribution within the radar resolution cell may become a large source of error when the attenuation is severe. A first-order correction to such effect is included in the algorithm. The validity of this nonuniform beam-filling correction method is yet to be verified. Nevertheless, some preliminary tests indicate that the attenuation-corrected radar reflectivity factors and rain estimates from this algorithm are statistically fairly reasonable.

An analysis of the parameter ϵ points to a significant difference between the characteristics of rain over the ocean and land. This finding indicates that rain over land may have a different drop size distribution or different structure than that of rain over the ocean. A future challenge will be to investigate whether a similar, but probably smaller, regional or seasonal difference exists over land or ocean.

Acknowledgments. We thank Dr. John Kwiatkowski for his timely assistance in running the experimental versions of the program at NASA's TRMM Science Data and Information System. We also thank Dr. Christian Kummerow for his continuous encouragement. The study was supported in part by the National Space Development Agency of Japan (NASDA).

APPENDIX

Derivation of the Nonuniform Beam-Filling Correction Factors

In this appendix, a two-dimensional nonuniformity problem is treated. We denote the probability distribution of the specific attenuation k within the radar resolution cell by $p(k)$. Let the mean of k be m_k and the variance be σ_k^2. Suppose that R and Z are related through $R = aZ^b$ and that k and Z are related through $k = \alpha Z^\beta$. Then $Z = \alpha' k^{1/\beta}$, where $\alpha' = \alpha^{-1/\beta}$. Similarly, R is related to k through $R = a(k/\alpha)^{b/\beta} = a\alpha'^b k^{b/\beta} = a_k k^{b_k}$.

We show the cases in which $p(k)$ is a gamma distribution and a lognormal distribution. Other types of distribution can also be assumed, but they generally need numerical integration to obtain the required relationships.

The gamma distribution with the mean m_k and the variance σ_k^2 can be expressed by using parameters $q = m_k^2/\sigma_k^2$ and $s = \sigma_k^2/m_k$ as

$$p(k) = F(k; q, s) = \frac{1}{\Gamma(q)s^q} k^{q-1} e^{-k/s} \quad \text{for } k > 0. \tag{A1}$$

From these relations, the averages of R and Z are

$$\langle R \rangle = a_k \int k^{b_k} p(k)\, dk = a_k \frac{\Gamma(b_k + q)}{\Gamma(q)} s^{b_k} = a\alpha'^b \frac{\Gamma(b/\beta + q)}{\Gamma(q)} s^{b/\beta} \quad \text{and} \tag{A2}$$

$$\langle Z \rangle = \alpha' \int k^{1/\beta} p(k)\, dk = \alpha' \frac{\Gamma(1/\beta + q)}{\Gamma(q)} s^{1/\beta}. \tag{A3}$$

Therefore, if we define a correction factor C_{RZ} by

$$\langle R \rangle = a\langle Z \rangle^b C_{RZ} \tag{A4}$$

then, C_{RZ} is given by

$$C_{RZ} = \frac{\Gamma(b/\beta + q)}{\Gamma(q)} \left[\frac{\Gamma(q)}{\Gamma(1/\beta + q)} \right]^b = \frac{\Gamma(b/\beta + m_k^2/\sigma_k^2)\Gamma^{b-1}(m_k^2/\sigma_k^2)}{\Gamma^b(1/\beta + m_k^2/\sigma_k^2)}. \tag{A5}$$

If a lognormal probability distribution is assumed instead, the probability density function has a form of

$$p(k) = \frac{1}{\sqrt{2\pi}\sigma k} \exp\left[-\frac{(\ln k - m)^2}{2\sigma^2} \right], \tag{A6}$$

where

$$m_k = e^{m + \sigma^2/2} \quad \text{and} \quad \sigma_k^2 = e^{2m+\sigma^2}(e^{\sigma^2} - 1). \tag{A7}$$

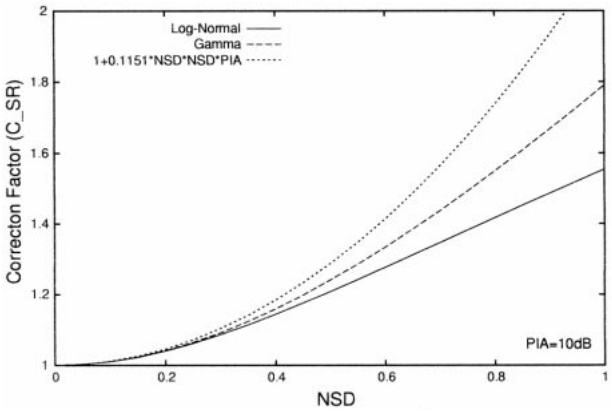

FIG. A1. Correction factor C_{SR} for the path-integrated attenuation as a function of σ_n when the apparent PIA is 10 dB. The solid line indicates the correction factor if the probability distribution of specific attenuation k follows the lognormal distribution. The broken line is for the gamma distribution, and the dotted line is the approximation formula used in the version-5.53 algorithm. In the actual algorithm, C_{SR} is set to 1.3 if C_{SR} is greater than 1.3.

With this probability distribution, we get

$$\langle R \rangle = a\alpha'^b e^{(mb/\beta) + (\sigma^2 b^2/2\beta^2)} \quad \text{and} \tag{A8}$$

$$\langle Z \rangle = \alpha' e^{(m/\beta) + (\sigma^2/2\beta^2)}. \tag{A9}$$

Therefore,

$$\langle R \rangle = a\langle Z \rangle^b e^{-b(1-b)\sigma^2/2\beta^2}. \tag{A10}$$

Because

$$1 + \frac{\sigma_k^2}{m_k^2} = e^{\sigma^2}, \tag{A11}$$

C_{RZ} can be expressed analytically as

$$C_{RZ} = \left(1 + \frac{\sigma_k^2}{m_k^2} \right)^{-b(1-b)/2\beta^2}. \tag{A12}$$

In both cases, if the normalized standard deviation defined by $\sigma_n = \sigma_k/m_k$ is small ($\sigma_n \ll 1$), the correction factor C_{RZ} can be approximated by

$$C_{RZ} \approx \frac{1}{1 + \dfrac{b(1-b)}{2\beta^2} \dfrac{\sigma_k^2}{m_k^2}} = \frac{1}{1 + \dfrac{b(1-b)}{2\beta^2} \sigma_n^2}. \tag{A13}$$

In the current version of 2A25, C_{RZ} is calculated by using

$$C_{RZ} = \frac{1}{1 + 0.2\sigma_n^2}, \tag{A14}$$

where the coefficient 0.2 in the denominator is an approximation to $b(1-b)/2\beta^2$.

Under the assumption that the ray approximation is valid, the attenuation factor to the surface at horizontal position $\mathbf{x}$ is

$$A(r_s, \mathbf{x}) = \exp\left[-0.2 \ln(10) \int_0^{r_s} k(s, \mathbf{x})\, ds \right]. \tag{A15}$$

In a case in which the horizontal nonuniformities at different vertical planes are similar to each other, that is, if the vertical profiles of k at different horizontal locations are similar to each other, then $k(r, \mathbf{x})$ can be expressed as a product of the normalized horizontal distribution $k_0(\mathbf{x})$ and the vertical profile of $m_k(r)$, which is the average of $k(r, \mathbf{x})$ over the horizontal plane at range r:

$$k(r, \mathbf{x}) = m_k(r)k_0(\mathbf{x}). \tag{A16}$$

By definition,

$$\int k_0(\mathbf{x})\, d\mathbf{x} = 1. \tag{A17}$$

In this case,

$$\int_0^{r_s} k(s, \mathbf{x})\, ds = k_0(\mathbf{x}) \int_0^{r_s} m_k(s)\, ds. \tag{A18}$$

Because $k_0(\mathbf{x})$ is normalized, if $p(k)$ follows a gamma distribution, $p(k_0)$ follows a gamma distribution with mean 1 and standard deviation σ_k/m_k that is constant from the assumption. Therefore, $qs = 1$, $qs^2 = \sigma_{k_0}^2/m_{k_0}^2 = \sigma_n^2$, and

$$p(k_0) = F\left(k_0; \frac{1}{\sigma_n^2}, \sigma_n^2\right) = \frac{1}{\Gamma(1/\sigma_n^2)\sigma_n^{2/\sigma_n^2}} k_0^{1/\sigma_n^2 - 1} e^{-k_0/\sigma_n^2}. \tag{A19}$$

Then, the average of $A(r_s)$ becomes

$$\langle A(r_s, \mathbf{x})\rangle = \int_0^\infty p(k_0) \exp\left[-0.2 \ln(10) k_0 \int_0^{r_s} m_k(s)\, ds\right] dk_0 = \int_0^\infty \frac{k^{1/\sigma_n^2 - 1}}{\Gamma(1/\sigma_n^2)\sigma_n^{2/\sigma_n^2}} \exp\left\{-k_0\left[\frac{1}{\sigma_n^2} + 0.2 \ln(10) \int_0^{r_s} m_k(s)\, ds\right]\right\} dk_0 = \frac{1}{\left[1 + 0.2 \ln(10)\sigma_n^2 \int_0^{r_s} m_k(s)\, ds\right]^{1/\sigma_n^2}}. \tag{A20}$$

On the other hand, the attenuation factor that would result if the same amount of rain were uniformly distributed is

$$A_u = \exp\left\{-0.2 \ln(10) \int_0^{r_s} \sigma\left[\frac{\langle R(s)\rangle}{a}\right]^{\beta/b} ds\right\}. \tag{A21}$$

Because

$$\langle R\rangle = a\alpha'^b \frac{\Gamma(b/\beta + q)}{\Gamma(q)} s^{b/\beta} = a\left(\frac{1}{\alpha}\right)^{b/\beta} \frac{\Gamma(b/\beta + m_k^2/\sigma_k^2)}{\Gamma(m_k^2/\sigma_k^2)} \left(\frac{\sigma_k^2}{m_k}\right)^{b/\beta} \tag{A22}$$

and σ_k/m_k is assumed to be constant irrespective of the vertical position,

$$A_u = \exp\left[-0.2 \ln(10) \frac{\Gamma^{\beta/b}(b/\beta + 1/\sigma_n^2)}{\Gamma^{\beta/b}(1/\sigma_n^2)} \sigma_n^2 \int_0^{r_s} m_k(s)\, ds\right]. \tag{A23}$$

The ratio $\ln(A_u)/\ln\langle A(r_s)\rangle$ is

$$\frac{\ln(A_u)}{\ln\langle A(r_s)\rangle} = \frac{0.2 \ln(10) \frac{\Gamma^{\beta/b}(b/\beta + 1/\sigma_n^2)}{\Gamma^{\beta/b}(1/\sigma_n^2)} \sigma_n^2 \int_0^{r_s} m_k(s)\, ds}{(1/\sigma_n^2) \ln\left[1 + 0.2 \ln(10)\sigma_n^2 \int_0^{r_s} m_k(s)\, ds\right]} = \frac{0.2 \ln(10)\Gamma^{\beta/b}(b/\beta + 1/\sigma_n^2)\sigma_n^4 \int_0^{r_s} m_k(s)\, ds}{\Gamma^{\beta/b}(1/\sigma_n^2) \ln\left[1 + 0.2 \ln(10)\sigma_n^2 \int_0^{r_s} m_k(s)\, ds\right]} = \frac{\Gamma^{\beta/b}(b/\beta + 1/\sigma_n^2)\sigma_n^4 P_u'}{\Gamma^{\beta/b}(1/\sigma_n^2) \ln(1 + \sigma_n^2 P_u')}. \tag{A24}$$

Here $P'_u = 0.2 \ln(10) \int_0^{r_s} m_k(s)\, ds = 0.1 \ln(10)\, \mathrm{PIA}_u$. In general, PIA_u is not necessarily small so that we cannot assume $\sigma_n^2 P'_u$ is small.

If the probability distribution is lognormal,

$$p(k_0) = \frac{1}{\sqrt{2\pi}\sigma k_0} \exp\left[-\frac{(\ln k_0 - m)^2}{2\sigma^2}\right], \quad \text{(A25)}$$

where

$$1 = e^{m+\sigma^2/2} \quad \text{and} \quad \frac{\sigma_k^2}{m_k^2} = \sigma_n^2 = (e^{\sigma^2} - 1), \quad \text{or} \quad \text{(A26)}$$

$$\sigma = \sqrt{\ln(1 + \sigma_n^2)} \quad \text{and}$$

$$m = -\frac{1}{2}\ln(1 + \sigma_n^2). \quad \text{(A27)}$$

Then, the average of $A(r_s)$ becomes

$$\begin{aligned}\langle A(r_s, \mathbf{x})\rangle &= \int_0^\infty p(k_0) \exp\left[-0.2 \ln(10) k_0 \int_0^{r_s} m_k(s)\, ds\right] dk_0 \\ &= \int_0^\infty \frac{1}{\sqrt{2\pi}\sigma k_0} \exp\left[-\frac{(\ln k_0 - m)^2}{2\sigma^2}\right] \exp\left[-0.2 \ln(10) k_0 \int_0^{r_s} m_k(s)\, ds\right] dk_0. \quad \text{(A28)}\end{aligned}$$

On the other hand, the attenuation factor that would result if the same amount of rain were uniformly distributed is

$$A_u = \exp\left\{-0.2 \ln(10) \int_0^{r_s} \alpha\left[\frac{\langle R(s)\rangle}{a}\right]^{\beta/b} ds\right\}. \quad \text{(A29)}$$

Because

$$\langle R\rangle = a\alpha'^b m_k^{b/\beta} \exp\left[\frac{\sigma^2 b}{2\beta}\left(\frac{b}{\beta} - 1\right)\right], \quad \text{(A30)}$$

$$A_u = \exp\left\{-0.2 \ln(10) \exp\left[\frac{\sigma^2}{2}\left(\frac{b}{\beta} - 1\right)\right] \int_0^{r_s} m_k(s)\, ds\right\}. \quad \text{(A31)}$$

The ratio $\ln(A_u)/\ln\langle A(r_s)\rangle$ is

$$\begin{aligned}\frac{\ln(A_u)}{\ln\langle A(r_s)\rangle} &= \frac{-0.2 \ln(10) \exp\left[\frac{\sigma^2}{2}\left(\frac{b}{\beta} - 1\right)\right] \int_0^{r_s} m_k(s)\, ds}{\ln\left\{\int_0^\infty \frac{1}{\sqrt{2\pi}\sigma k_0} \exp\left[-\frac{(\ln k_0 - m)^2}{2\sigma^2}\right] \exp\left[-0.2 \ln(10) k_0 \int_0^{r_s} m_k(s)\, ds\right] dk_0\right\}} \\ &= \frac{-e^{(\sigma^2/2)(b/\beta - 1)} P'_u}{\ln\left\{\int_0^\infty \frac{1}{\sqrt{2\pi}\sigma k_0} \exp\left[-\frac{(\ln k_0 - m)^2}{2\sigma^2} - k_0 P'_u\right] dk_0\right\}} \\ &= \frac{-(1 + \sigma_n^2)^{[(b/\beta)-1]/2} P'_u}{\ln\left\{\frac{1}{\sqrt{2\pi \ln(1 + \sigma_n^2)}}(1 + \sigma_n^2)^{-1/8} \int_{-\infty}^\infty \exp\left[-\frac{y^2}{2 \ln(1 + \sigma_n^2)} - \frac{1}{2}y - P'_u e^y\right] dy\right\}}. \quad \text{(A32)}\end{aligned}$$

In both the gamma and lognormal cases, the correction factor for attenuation $C_{\mathrm{SR}} = \ln(A_u)/\ln\langle A(r_s)\rangle$ can be estimated only by a numerical method. Unlike the correction factor for Z–R relation that depends only on the normalized standard deviation σ_n, the correction factor for attenuation C_{SR} depends on the total path-integrated attenuation as well.

Figure A1 shows the dependence of C_{SR} as a function of σ_n for PIA = 10 dB. When $\sigma_n \ll 1$ and $\sigma_n^2 P'_u \ll 1$, a first order approximation to (A24) and (A32) becomes

$$C_{\mathrm{SR}} = 1 + \frac{1}{2}\left(P'_u + \frac{b}{\beta} - 1\right)\sigma_n^2. \quad \text{(A33)}$$

Because $b/\beta \approx 1$, C_{SR} is calculated by a crude approximation formula of

$$C_{SR} = 1 + c_1 \sigma_n^2 \text{PIA} \quad \text{(A34)}$$

in 2A25, where the coefficient c_1 is chosen to be 0.115 [$=0.05$ ln(10)]. This formula gives an overestimate when σ_n^2PIA is not small. However, when we think about the error in the estimate of σ_n^2, the error caused by this approximation is small in comparison with the uncertainty in σ_n itself. Furthermore, whenever C_{SR} is larger than the threshold value (which is currently set to 1.3), C_{SR} is reset to this threshold value. Therefore, the approximation formula is used only for the narrow range of variable in which the approximation is not very different from the exact formula. A large value of C_{SR} is forbidden to avoid an unrealistically large attenuation correction from the fluctuation of estimated σ_n. Possible further improvements, including a three-dimensional nonuniform beam-filling correction are under investigation.

REFERENCES

Ajayi, G. O., and I. E. Owolabi, 1987: Rainfall parameters from disdrometer dropsize measurements at a tropical station. *Ann. Telecomm.,* **42,** 3–12.

Amayenc, P., J. P. Diguet, M. Marzoug, and T. Tani, 1996: A class of single- and dual-frequency algorithms for rain-rate profiling from a spaceborne radar. Part II: Tests from airborne radar measurements. *J. Atmos. Oceanic Technol.,* **13,** 142–164.

Austin, P. M., and S. G. Geotis, 1979: Raindrop sizes and related parameters for GATE. *J. Appl. Meteor.,* **18,** 569–575.

Awaka, J., Y. Furuhama, M. Hoshiyama, and A. Nishitsuji, 1985: Model calculations of scattering properties of spherical bright-band particles made of composite dielectrics. *J. Radio Res. Lab.,* **32,** 73–87.

Cunning, J. B., and I. Sax, 1977: A *Z–R* relationship for the GATE B-scale array. *Mon. Wea. Rev.,* **105,** 1330–1336.

Foote, G. B., and P. S. du Toit, 1969: Terminal velocity of raindrops aloft. *J. Appl. Meteor.,* **8,** 249–253.

Hardy, G., J. E. Littlewood, and G. Pólya, 1952: *Inequalities.* Cambridge University Press, 324 pp.

Hitschfeld, W., and J. Bordan, 1954: Errors inherent in the radar measurement of rainfall at attenuating wavelengths. *J. Meteor.,* **11,** 58–67.

Iguchi, T., and R. Meneghini, 1994: Intercomparison of single-frequency methods for retrieving a vertical rain profile from airborne or spaceborne radar data. *J. Atmos. Oceanic Technol.,* **11,** 1507–1516.

Kozu, T., and T. Iguchi, 1999: Nonuniform beamfilling correction for spaceborne radar rainfall measurement: Implications from TOGA COARE radar data analysis. *J. Atmos. Oceanic Technol.,* **16,** 1722–1735.

——, ——, K. Shimizu, and N. Kashiwagi, 1999: Estimation of raindrop size distribution parameters using statistical relations between multiparameter rainfall remote sensing data. Preprints, *29th Int. Conf. on Radar Meteorology,* Montreal, Quebec, Canada, Amer. Meteor. Soc. 689–692.

Kummerow, C., and Coauthors, 2000: The status of the Tropical Rainfall Measuring Mission (TRMM) after two years in orbit. *J. Appl. Meteor.,* **39,** 1965–1982.

Marzoug, M., and P. Amayenc, 1994: A class of single- and dual-frequency algorithms for rain-rate profiling from a spaceborne radar. Part I: Principle and tests from numerical simulations. *J. Atmos. Oceanic Technol.,* **11,** 1480–1506.

Meneghini, R., J. Eckerman, and D. Atlas, 1983: Range profiling of the rain rate by an airborne weather radar. *Remote Sens. Environ.,* **31,** 193–209.

——, T. Iguchi, T. Kozu, L. Liao, K. Okamoto, J. A. Jones, and J. Kwiatkowski, 2000: Use of the surface reference technique for path attenuation estimates from the TRMM Precipitation radar. *J. Appl. Meteor.,* **39,** 2053–2070.

Nishitsuji, A., M. Hoshiyama, J. Awaka, and Y. Furuhama, 1983: An analysis of propagation character at 34.5 GHz and 11.5 GHz between *ETS-II* satellite and Kashima station—On the precipitation model from stratus (in Japanese). *Trans. IECE Japan,* **66B,** 1163–1170.

Short, D. A., T. Kozu, and K. Nakamura, 1990: Rain rate and raindrop size distribution observations in Darwin, Australia. *Proc. Special Symp. on Regional Factors Affecting Radiowave Attenuation due to Rain,* Rio de Janeiro, Brazil, International Union of Radio Science Commission, 35–40.

Simpson, J., and Coauthors, 2000: The Tropical Rainfall Measuring Mission (TRMM) progress report. *Earth Observ. Remote Sens.,* in press.

Stout, G. E., and E. A. Mueller, 1968: Survey of relationships between rainfall rate and radar reflectivity in the measurement of precipitation. *J. Appl. Meteor.,* **7,** 465–474.

Tokay, A., and D. A. Short, 1996: Evidence from tropical raindrop spectra of the origin of rain from stratiform versus convective clouds. *J. Appl. Meteor.,* **35,** 355–371.